Microwave Photonic Pulse Generation With High Transfer Rate and Precision Pulse Width by Partly Temporally-Overlapped Photon Echo Excitation

Xiangrong Wang, Shuanggen Zhang, Jinlei Liu, and Shumin Wang

***Abstract*—Microwave photonic pulse generation has intrinsic high speed and large bandwidth, and it can overcome the sampling-rate limitation in the electrical domain. Herein, we propose a partly temporally-overlapped photon echo scheme to generate microwave pulses with a high data transfer rate and precision pulse width. The partly overlapped chirped control pulse has the same chirped rate segments but different time delays. The time delay between the segments and the number of segments can be adjusted to achieve a controllable multipulse photon echo train. We developed a theoretical model based on the photon echo process and performed simulations to obtain nonlinear chirped periodic spectral grating in a Tm^{3+}:YAG crystal and gave the time delay provided by the spectral grating to the probe pulse at different instantaneous frequencies. We further generated pulse code modulation signals to verify the performance of the target signal. The proposed signal-generation scheme has potential applications in microwave photonics and modern radar systems.**

***Index Terms*—Photon echo, spectral grating, optical arbitrary waveform generators, rare-Earth-doped crystal.**

I. Introduction

PHOTONIC generation of microwave waveform signal has recently become an engaging research area due to its utilization in optical communication and all-optical microwave signal processing systems [1]–[4]. The optical arbitrary waveform generators (OAWGs) offers high speed, low complexity and low power consumption at high bandwidths compared to its electrical counterpart [5]. Optical arbitrary signals can be conventionally generated by direct space-time (DST) pulse shaping, temporal pulse shaping (TPS) based on Mach–Zendel modulator and dispersive elements, spectral shaping, and frequency-to-time mapping [6]–[8]. Nevertheless, the above methods usually generate time-bandwidth products from a few tens to a few hundred. At present, an arbitrary signal generation scheme based on photon echoes can generate several narrow photon echo pulses with controllable amplitudes and intervals by incident multiple probe or control pulses to compose the target signal [9]–[12]. With the large inhomogeneous broadening absorption line of tens of GHz provided by Tm^{3+}:YAG crystals, the time-bandwidth product can reach 10^5 [13], however, it employs a frequency shift to generate a photon echo train, which reduces the subpulse-width accuracy. Herein, we proposed the optical synthesis of microwave signals via photon echo pulse train with the variable amplitude and adjustable time delay generated by partly temporally-overlapped excitation and segmented control pulses, which can offer high precision subpulse width of photon echo signals while maintaining a high data transfer rate and provides a more flexible bandwidth consumption.

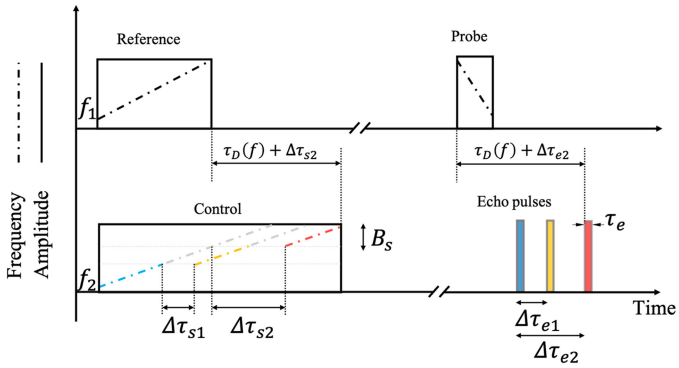

Fig. 1. Pulse sequence configuration of temporally partly overlapped photon echoes.

II. Principle And Theoretical Description

A different optical synthesis scheme of microwave signals is proposed. The pulse sequence based on a segmented control pulse employed to generate multiple compressed photon echoes is shown in Fig. 1, where the reference and control chirp pulses are temporally partly overlapped. However, they have different chirp rates and initial frequencies of α_1, f_1, and α_2, f_2, respectively. The Tm^{3+}:YAG crystal is excited by the two chirped pulses, whereas a spectral grating with a nonlinear chirped periodic structure is engraved in its inhomogeneous broadening absorption line, which provides a different time delay $\tau_D(f)$ at different instantaneous frequency components of the input chirped probe pulse to form a compressed photon echo with a time-width τ_e. Furthermore, τ_e is approximately equal to the

Manuscript received October 15, 2021; revised November 26, 2021; accepted December 16, 2021. Date of publication December 20, 2021; date of current version January 12, 2022. This work was supported in part by the Natural Science Foundation of Tianjin under Grant 19JCYBJC16100, and in part by the Tianjin Research Innovation Project for Postgraduate Students under Grant 2020YJSS165. *(Corresponding author: Shuanggen Zhang).*

The authors are with the Tianjin Key Laboratory of Film Electronic and Communication Device, School of Integrated Circuit Science and Engineering, Tianjin University of Technology, Tianjin 300384, China (e-mail: wangxr12138@gmail.com; shuanggenzhang@163.com; 1412923869@qq.com; 18482286575@163.com).

Digital Object Identifier 10.1109/JPHOT.2021.3136669

reciprocal of the bandwidth B, which is the frequency-domain overlapping of the three pulses. Compared with the frequency shift scheme in Ref. [9] and [13], the proposed photon echo scheme can achieve a variable echo pulse width τ_e by adjusting the bandwidth of the corresponding segment of the control pulse. And to generate a compressed photon echo, the chirp rate of the pulse sequence must conform to the relationship $\alpha_3 = \alpha_1\ \alpha_2/(\alpha_2 - \alpha_1)$, where α_3 is the chirp rate of the probe pulse. Notably, the inhomogeneous broadening absorption line bandwidth limits the maximum overlapping bandwidth, i.e., $B_{max} \leq B_{inh}$. For Tm^{3+}:YAG crystal $B_{inh} \approx 40\ GHz$. The light-dashed line in Fig. 1 represents the extension of the instantaneous frequency.

The reference, segmented control, and probe pulses are expressed by (1)–(3), respectively, where $A_n,\ (n\ =\ 1, 2, 3)$ is the amplitude.

$$E_1(t) = A_1 e^{i2\pi\left(f_{s1}t + \frac{1}{2}\alpha_1 t^2\right)} \tag{1}$$

$$E_2(t) = \begin{cases} E_2'(t) = A_2 e^{i2\pi\left(f_{s2}t + \frac{1}{2}\alpha_2 t^2\right)} & t_1 < t < t_1' \\ E_2''(t) = A_2 e^{i2\pi\left[f_{s2}(t-\Delta\tau_{s1}) + \frac{1}{2}\alpha_2(t-\Delta\tau_{s1})^2\right]} & t_2 < t < t_2' \\ E_2'''(t) = A_2 e^{i2\pi\left[f_{s2}(t-\Delta\tau_{s2}) + \frac{1}{2}\alpha_2(t-\Delta\tau_{s2})^2\right]} & t_3 < t < t_3' \end{cases} \tag{2}$$

$$E_3(t) = A_3\ e^{i2\pi\left(f_{s3}t + \frac{1}{2}\alpha_3 t^2\right)} \tag{3}$$

The spectral grating $G(f)$ can be expressed as $G(f) = E_1^*(f)E_2(f)$ from the Fourier transform of (1) and (2). As the probe pulse interacts with the crystal, each instantaneous frequency component has a time delay $\tau_D(f) = f(1/\alpha_2 - 1/\alpha_1) - f_2/\alpha_2 + f_1/\alpha_1$ provided by the spectral grating, which acts as a filter. The delay makes all the frequency components simultaneously leave the spectral grating to form compressed photon echoes. However, the case is different when using segmented control pulses. The time delay provided to the probe pulse by the spectral grating formed by the first segment control pulse remains $\tau_D(f)$, but that provided by the second and third segments is $\tau_D(f) + \Delta\tau_{s1}$ and $\tau_D(f) + \Delta\tau_{s2}$, respectively. Based on the three time delays, we obtain the time interval for each photon echo $\Delta\ \tau_{e1} = \tau_D\ (f) + \Delta\tau_{s1} - \tau_D\ (f) = \Delta\tau_{s1}$and $\Delta\ \tau_{e2} = \tau_D\ (f) + \Delta\tau_{s2} - \tau_D\ (f) = \Delta\tau_{s2}$. It is worth noting that $\tau_D(f) + \Delta\tau_{sk} (k\ =\ 0, 1, 2, \ldots, n,\ \Delta\ \tau_{s0} = 0)$ should be less than the transverse relaxation time $T_2 = 10\mu s$ of the Tm^{3+}:YAG crystal. By applying segmented control pulses, photon-echo pulse width errors caused by frequency shifts generating multiple compressed pulses can be prevented. The three compressed photon echoes with different time delays can be expressed by (4)–(6), which are obtained from the Fourier inversion of $G(f)E_3(f)$. In these equations, $f_{c1} = f_1\ + B/2$, $f_{c2} = f_1\ + B + B/2\ = f_1\ + 3B/2$, $f_{c3} = f_1\ + 2B + B/2\ = f_1\ + 5B/2$, and $E_n(f)$ is the Fourier transform of $E_n(t)$, $(n\ =\ 1,\ 2,\ 3)$.

$$E_{cp1}(t) \propto \int_{f_{c1}-B/2}^{f_{c1}+B/2} E_1^*(f)E_2(f)\,E_3(f)\,e^{i2\pi ft}df$$
$$\propto e^{i2\pi f_{c1}\left[t - \frac{f_{s1}}{\alpha_1} + \frac{f_{s2}}{\alpha_2} + \frac{f_{s3}}{\alpha_3}\right]}$$
$$\cdot\ sinc\left[B\pi\left(t - \frac{f_{s1}}{\alpha_1} + \frac{f_{s2}}{\alpha_2} + \frac{f_{s3}}{\alpha_3}\right)\right] \tag{4}$$

$$E_{cp2}(t) \propto \int_{f_{c2}-\frac{B}{2}}^{f_{c2}+\frac{B}{2}} E_1^*(f)E_2(f)\,E_3(f)\,e^{i2\pi f(t-\Delta\tau_{s1})}df$$
$$\propto e^{i2\pi f_{c2}\left[(t-\Delta\tau_{s1}) - \frac{f_{s1}}{\alpha_1} + \frac{f_{s2}}{\alpha_2} + \frac{f_{s3}}{\alpha_3}\right]}$$
$$\times\ sinc\left[B\pi\left((t-\Delta\tau_{s1})\ - \frac{f_{s1}}{\alpha_1} + \frac{f_{s2}}{\alpha_2} + \frac{f_{s3}}{\alpha_3}\right)\right]$$
$$= E_{cp1}(t - \Delta\tau_{s1}) \tag{5}$$

$$E_{cp3}(t) \propto \int_{f_{c3}-\frac{B}{2}}^{f_{c3}+\frac{B}{2}} E_1^*(f)E_2(f)\,E_3(f)\,e^{i2\pi f(t-\Delta\tau_{s2})}df$$
$$\propto e^{i2\pi f_{c3}\left[(t-\Delta\tau_{s2}) - \frac{f_{s1}}{\alpha_1} + \frac{f_{s2}}{\alpha_2} + \frac{f_{s3}}{\alpha_3}\right]}$$
$$\times\ sinc\left[B\pi\left((t-\Delta\tau_{s2})\ - \frac{f_{s1}}{\alpha_1} + \frac{f_{s2}}{\alpha_2} + \frac{f_{s3}}{\alpha_3}\right)\right]$$
$$= E_{cp1}(t - \Delta\tau_{s2}) \tag{6}$$

The general photon echo is expressed by (7), where $f_{ci} = f_1\ + (i-1)B + B/2,\ \ i\ = (1, 2, 3, \ldots, n), \Delta\tau_{s0} = 0$, and E_{cp1} represents the first photon echo.

$$E_{cpi}(t) \propto e^{i2\pi f_{ci}\left[\left(t-\Delta\tau_{s(i-1)}\right) - \frac{f_{s1}}{\alpha_1} + \frac{f_{s2}}{\alpha_2} + \frac{f_{s3}}{\alpha_3}\right]}$$
$$\times\ sinc\left[B\pi\left(t - \Delta\tau_{s(i-1)}\right) - \frac{f_{s1}}{\alpha_1} + \frac{f_{s2}}{\alpha_2} + \frac{f_{s3}}{\alpha_3})\right]$$
$$= E_{cp1}\ \left(t - \Delta\tau_{s(i-1)}\right) \tag{7}$$

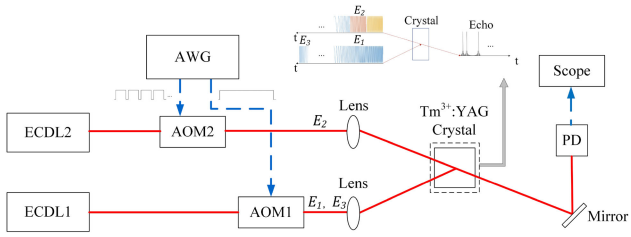

Fig. 2. Schematic of generating multiple compressed photon echoes. ECDL: external cavity diode laser; AWG: arbitrary waveform generator; AOM: acousto-optic modulator; BS: beam splitter; PD: photodetector.

Fig. 2 shows the schematic of the proposed photon echo scheme, which indicates the time sequence, modulation method and directional relationship between $E_1(t)$, $E_2(t)$ and $E_3(t)$ in the simulation process. The red and blue lines indicate the optical and electrical paths, respectively. AWG, AOM1, and AOM2 modulate the two beams generated by ECDL1 and ECDL2 to produce $E_1(t)$ and $E_2(t)$ with chirp rate α_1 and α_2, respectively. When $E_1(t)$ and $E_2(t)$ are focused onto the cryogenically cooled Tm^{3+}:YAG crystal at a certain angle, spectral grating is generated in the inhomogeneous broadening absorption line. Then, $E_3(t)$ with a chirp rate α_3 is generated by AWG, AOM1, and ECDL1. As the probe pulse is focused onto the crystal after a short time delay, the photon echo signal is detected by PD and displayed by the scope. The direction relationship between the

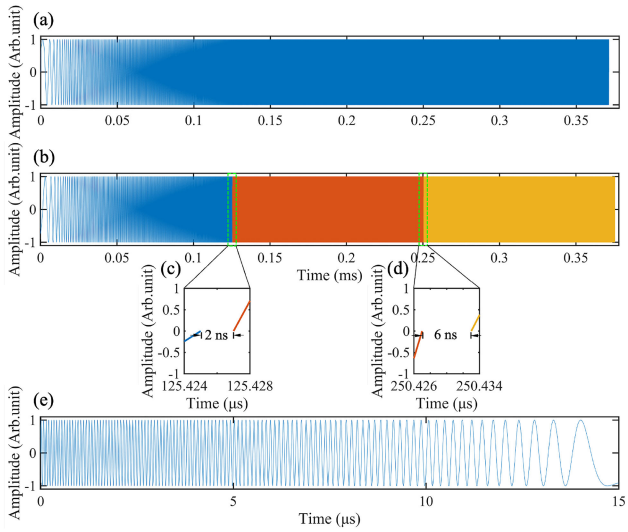

Fig. 3. Incident pulse waveform of photon echo scheme based on segmented control pulses: (a) Reference pulse; (b) Segmented control pulse; (c) and (d) Enlarged images of the areas in the green dotted line frame in (b). The interval between the first and second segments is 2 ns, and that between the second and third segments is 6 ns. (e) Probe pulse.

three incident pulses and the photon echoes is represented in the subplot of the dashed box in Fig. 2.

III. Period of Spectral Grating and Time Interval Control

The period of spectral grating determines the time delay provided to the detection pulse. Following the signal generation procedure (Fig. 1), we generated three compressed photon echo signals with intervals $\Delta\,\tau_{e1} = 2ns$ and $\Delta\,\tau_{e2} = 6ns$ to obtain and analyze the structure of the spectral grating. The waveforms of the incident pulse sequence are shown in Fig. 3. In particular, the control pulse takes the form of segments and, according to the equation $\Delta\,\tau_s = \Delta\tau_e$, we have $\Delta\,\tau_{s1} = 2ns$ and $\Delta\,\tau_{s2} = 6ns$. $E_1(t)$, $E_2(t)$ and $E_3(t)$used in the paper have normalized magnitudes, i.e., $A_3 = A_2 = A_3 = 1$. We set $B = 5\,GHz$, and the durations of the temporally partly overlapped linear frequency-chirped pulses are 371.29 and 375.43, and 15 μs for the probe pulse, respectively. The chirp rates of the three pulses are $\alpha_1 = 4.04 \times 10^{13} Hz/s$, $\alpha_2 = 4 \times 10^{13}\ Hz/s$, $\alpha_3 = 1 \times 10^{15}\ Hz/s$, with the start frequencies $f_1 = 80\ MHz$, $f_2 = 63\ MHz$, and $f_3 = 15.08\ GHz$, respectively. In practical situations, the chirp rates can be achieved by an external cavity diode laser (ECDL) with a tunable range up to tens of GHz.

Fig. 4(a) shows the spectral grating generated in the Tm^{3+}:YAG crystal by temporally partly overlapped linear frequency-chirped pulses shown in Figs. 3(a) and (b). In Figs. 4(b)–(g), the period of the spectral grating decreases from 2.35 to 241.2 kHz with as the instantaneous frequency in the form of a nonlinear chirp increases. Conversely, because the time delay $\tau_D(f)$ provided by spectral grating is the reciprocal of the grating's period at f, $\tau_D(f)$ increases as the period decreases.

The red line in Fig. 5 shows the nonlinear chirped structure of the spectral grating period with abrupt changes at 5.08 and 10.08 GHz. With the abrupt change, we could achieve multiple compressed photon echoes using a single segmented control pulse, which could only be produced with multiple frequency-shifted control or probe pulses in previous designs. Moreover, the data on the blue line are obtained from the reciprocal of the data of the red line, and the two abrupt changes of 2 and 6 ns obtained at 5.08 and 10.08 GHz correspond to Fig. 4(h).

IV. Pulse Code Modulation Signal Generation Based on Segmented Control Pulse

The temporally arbitrary pulse shapes can be synthesized via programming the amplitude and time delay of the subpulse train generated by the proposed photon echo scheme. As one of the essential coding methods in digital communication, pulse code modulation (PCM) signal is an appropriate target signal to manifest the unique advantages of the optical synthesis scheme of microwave signals. PCM signals are precisely binary sequences obtained by sampling, quantizing, and encoding discrete intervals of analog signals [14], [15]. Suppose the data of a PCM signal is $a = \{a_1, a_2, \ldots, a_n\}$, then each segment of the control pulse is used to generate a_k, $(k = 1, 2, 3, \ldots, n)$, and the first segment of the control pulse is used to determine the beginning time of the photon echo. The time delay between the first and the kth pulse is given by

$$\Delta\,\tau_k = k \cdot\ \tau_e = \frac{k}{B} \tag{8}$$

As shown in Fig. 6, a PCM signal (0, 0, 1, 1, 1, 0, 0, 1, 0, 1, 0, 0, 0, 1, 0, 1) with a transfer rate of 5 $Gbit/s$, a time width of 4 ns and a bandwidth of 40 *GHz* with an 80 *MHz* starting frequency is produced with the configuration described in Fig. 1. τ_e of each photon echo pulse in the PCM signal is 0.2 ns. The reference and control pulse durations are 0.9901 and 1.00044 ms, respectively, and that of the probe pulse is 40 μs. The data show that seven compressed photon echo should be produced on behalf of the "1", and a positioning photon echo is needed to determine the starting position of the subpulse train. Then, the interval $\Delta\tau_k$ between the first and the seven compressed photon echoes is 0.6, 0.8, 1, 1.6, 2, 2.8, and 3.2 ns, respectively, according to (7). Therefore, setting the bandwidth of each section of the control pulse to 5 *GHz*, the total bandwidth of the eight sections is 40 *GHz*. The chirp rates of the pulse sequence are $\alpha_1 = 4.04 \times 10^{13} Hz/s$, $\alpha_2 = 4 \times 10^{13}\ Hz/s$, and $\alpha_3 = 1 \times 10^{15}\ Hz/s$, respectively, and the starting frequencies are $f_1 = 80\ MHz$, $f_2 = 63\ MHz$, and $f_3 = 40.08\ GHz$.

The data transfer rate in a signal generation system is an important performance parameter. Fig. 7 shows the change in the data transfer rate of PCM signal with the number of segments at different bandwidth limits. The data transfer rate is proportional to the bandwidth and inversely proportional to the number of generated pulses. Although the data transfer rate decreases as the number of pulses increases, the individual data lines converge at ~1 *Gbit/s*. However, as the inhomogeneous broadening absorption line provided by the crystal material increases to

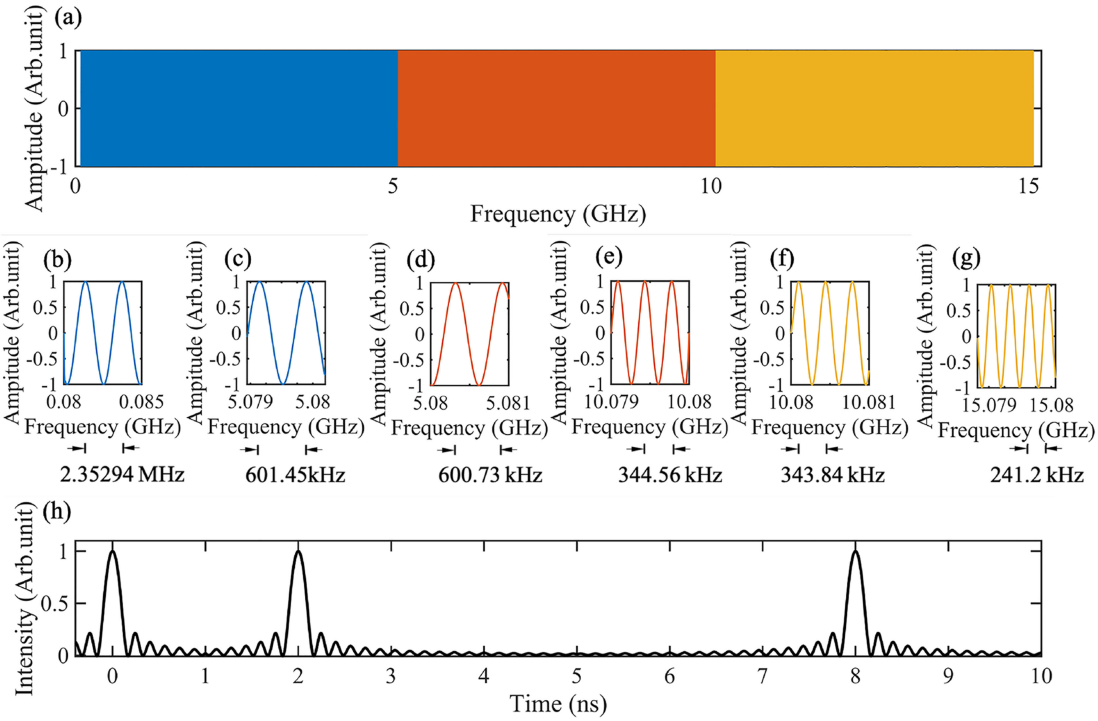

Fig. 4. Spectral grating structure and generated photon echo pulses: (a) Structure of the entire spectral grating. (b)–(g) Changes in the period of the spectral grating when the beginning and end of each segment of the spectral grating are magnified. When the detection pulse shown in (e) is incident on the crystal of the spectral grating, as shown in (a), in the inhomogeneous broadening absorption line, the photon echo signal as shown in (h) is obtained. The delay between pulses is 2 ns and 6 ns, respectively.

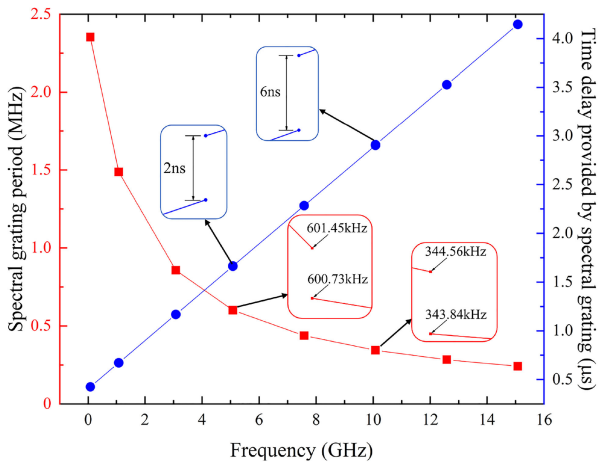

Fig. 5. Spectral grating period and the time delay it provides versus instantaneous frequency.

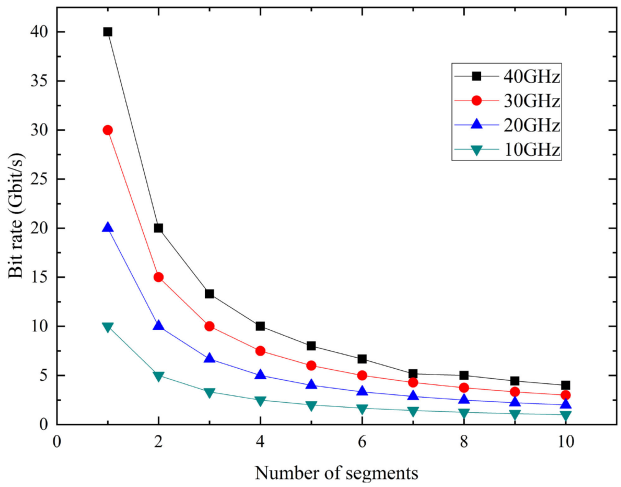

Fig. 7. Data transfer rate versus the number of segments at different bandwidth limits.

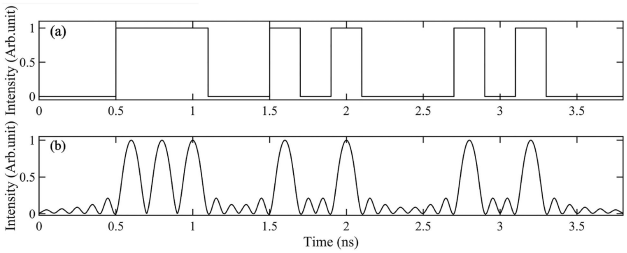

Fig. 6. Simulation for the PCM signal with data sequence of "00111001010000101": (a) Target PCM signal; (b) Generated PCM signal.

hundreds of *GHz*, the data transfer rate of the signal generated by this scheme increases, reaching tens of *Gbit/s*.

Fig. 8 compares the echo pulse width errors of the segmented and frequency-shifted models [9] (red and black data points, respectively) in generating a photon echo train with $\tau_e \approx 1/B$ of 5 *ns* and $\Delta\tau_e$ of 15 *ns*. The frequency shift model generates multiple echoes by frequency shifting $\Delta f = \alpha_2 \Delta\tau_e$ of the control pulse which reduces the overlap bandwidth B of $E_1(t)$, $E_2(t)$, $E_3(t)$ and therefore increases the echo pulse width. In

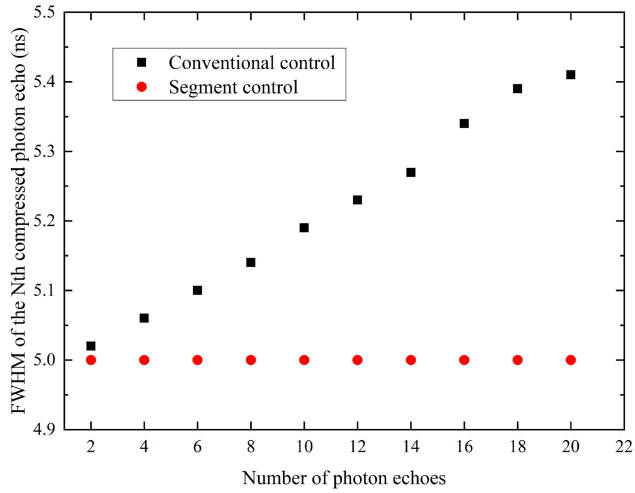

Fig. 8. Pulse width versus the number of photon echoes by the segmented control pulse compared to the frequency-shift method.

the case of the frequency-shifted model, with an increase in the number of photon echoes, the pulse width increases from 5 to 5.4 *ns*. In order to generate the second photon echo, the control pulse frequency shift Δf is required, and the overlapping bandwidth $B^{'} = B - \Delta f$. Then, the pulse width of the second compressed photon echo $\tau_{e2} \approx 1/(B - \Delta f)$. If the frequency shift between each control pulse is the same, the pulse width of the *n*th compressed photon echo $\tau_{en} \approx 1/(B - (n-1)\Delta f)$. Hence, the error value is $\tau_{en} - \tau_{e1}$. According to the function, the more the compressed photon echoes generated, the greater the error of the pulse width in the frequency shift model. However, different to Ref. [9] and [13], the proposed optical synthesis scheme of microwave signals has the capability to eliminate the subpulse width errors caused by frequency shifts, since the partly temporally-overlapped excitation and segmented control pulses are applied and the overlapping bandwidth of each segment is the same. The theoretical analysis and simulation results given in the paper verified the excellent performance of the proposed optical synthesis scheme of microwave signal.

V. Conclusion

Herein, we developed a microwave photonic-pulse generation method based on partly overlapping photon echo with a high bit rate and precision pulse width. The variable time delay $\Delta\tau_e$ between multiple compressed photon echoes is determined by the segment delay $\Delta\tau_s$ of the partly overlapping chirped pulse; thus, a pulse train is achieved. Considering the partly overlapping chirped-pulse configuration, we developed a theoretical model based on the photon echo process and simulated the model to obtain chirped periodic spectral grating in a Tm^{3+}:YAG crystal. Different time delays were obtained at different frequency components provided to the input chirped pulse. We obtained a PCM target signal, which achieves a data transfer rate of the magnitude of *Gbit/s* and maintains a nearly error-free subpulse width. Notably, the echo efficiency may need to be optimized in the practical experiment to achieve the synthesized waveforms as expected. Also, waveform deterioration may also occur under a fast chirp rate [17]. The signal generation scheme may offer potential applications in ultra wide band (UWB) communication owning to the large bandwidth and high transfer rate. The method would pave a way for signal generation in microwave photonics and modern radar systems.

References

[1] J. Hu, J. Li, J. Zhao, Z. Ren, Y. Gu, and M. Zhao, "A simple scheme for photonic generation of microwave waveforms using a dual-drive Mach–Zehnder modulator," *Appl. Sci.*, vol. 10, no. 21, Nov. 2020, Art. no. 7914.

[2] M. Shin and P. Kumar, "Optical microwave frequency up-conversion via a frequency-doubling optoelectronic oscillator," *IEEE Photon. Technol. Lett.*, vol. 19, no. 21, pp. 1726–1728, Nov. 2007.

[3] A. I. Latkin, S. Boscolo, R. S. Bhamber, and S. K. Turitsyn, "Doubling of optical signals using triangular pulses," *J. Opt. Soc. Amer. B*, vol. 26, no. 8, pp. 1492–1496, Aug. 2009.

[4] R. S. Bhamber, A. I. Latkin, S. Boscolo, and S. K. Turitsyn, "All-optical TDM to WDM signal conversion and partial regeneration using XPM with triangular pulses," in *Proc. 34th Eur. Conf. Opt. Commun.*, Brussels, Belgium, 2008, pp. 1–2.

[5] K. Singh, J. Meier, A. Misra, S. Preußler, J. C. Scheytt, and T. Schneider, "Photonic arbitrary waveform generation with three times the sampling rate of the modulator bandwidth," *IEEE Photon. Technol. Lett.*, vol. 32, no. 24, pp. 1544–1547, Dec. 2020.

[6] J. D. McKinney, D. E. Leaird, and A. M. Weiner, "Millimeter-wave arbitrary waveform generation with a direct space-to-time pulse shaper," *Opt. Lett.*, vol. 27, no. 15, pp. 1345–1347, Aug. 2002.

[7] M. Li, C. Wang, W. Li, and J. Yao, "An unbalanced temporal pulse-shaping system for chirped microwave waveform generation," *IEEE Trans. Microw. Theory Techn.*, vol. 58, no. 11, pp. 2968–2975, Nov. 2010.

[8] W. Zhang and J. Yao, "Silicon-based on-chip electrically-tunable spectral shaper for continuously tunable linearly chirped microwave waveform generation," *J. Lightw. Technol.*, vol. 34, no. 20, pp. 4664–4672, Oct. 2016.

[9] Z. W. Barber, M. Tian, R. R. Reibel, and W. R. Babbitt, "Optical pulse shaping using optical coherent transients," *Opt. Exp.*, vol. 10, no. 20, pp. 1145–1150, Oct. 2002.

[10] R. R. Reibel, T. Chang, M. Tian, and W. R. Babbitt, "Optical linear sideband chirp compression for microwave arbitrary waveform generation," in *Proc. IEEE Int. Topical Meeting Microw. Photon.*, Ogunquit, ME, USA, 2004, pp. 197–200.

[11] C. J. Renner, R. R. Reibel, M. Tian, T. Chang, and W. R. Babbitt, "Broadband photonic arbitrary waveform generation based on spatial-spectral holographic materials," *J. Opt. Soc. Amer. B*, vol. 24, no. 12, pp. 2979–2987, Dec. 2007.

[12] V. Damon, V. Crozatier, T. Chanelière, J. L. L. Gouët, and I. Lorgeré, "Broadband photonic arbitrary waveform generation using a frequency agile laser at 15 μm," *JOSA B*, vol. 27, no. 3, pp. 524–530, Mar. 2010.

[13] X. Ma, S. Wang, Y. Liang, and Y. Shan, "High time–bandwidth product and high repetition rate period signal generation based on spectral hole burning crystal," *Appl. Opt.*, vol. 54, no. 10, pp. 2891–2896, Apr. 2015.

[14] J. F. Norris and D. F. Lovely, "Real-time compression of myoelectric data utilising adaptive differential pulse code modulation," *Med. Biol. Eng. Comput.*, vol. 33, no. 5, pp. 629–635, Sep. 1995.

[15] D. H. Whalen, E. R. Wiley, P. E. Rubin, and F. S. Cooper, "The Haskins Laboratories' pulse code modulation (PCM) system," *Behav. Res. Methods, Instruments, Comput.*, vol. 22, no. 6, pp. 550–559, Nov. 1990.

[16] H. Zhang, S. Zhang, S. Li, and X. Ma, "Performance analysis of double-amplitude population gratings by non-overlapping unipolar pulses," *Opt. Commun.*, vol. 462, May 2020, Art. no. 125182.

[17] T. Chang, M. Tian, R. K. Mohan, C. Renner, K. D. Merkel, and W. R. Babbitt, "Recovery of spectral features readout with frequency-chirped laser fields," *Opt. Lett.*, vol. 30, no. 10, pp. 1129–1131, May 2005.